remote sensing

MDPI

Article

Research on Inversion and Correction Method of Urban Light Environment Based on Cooperative Observation

Baogang Zhang [1], Yiwei Li [2], Ming Liu [2,*], Yuchuan Liu [2], Tong Luo [2], Qingyuan Liu [2], Lie Feng [2] and Weili Jiao [3]

[1] Laboratory of Building Environment and New Energy Resources, Faculty of Infrastructure Engineering, Dalian University of Technology, Dalian 116000, China; zhangbaogang@dlut.edu.cn
[2] School of Architecture and Fine Art, Dalian University of Technology, Dalian 116000, China; liyiweilizy@mail.dlut.edu.cn (Y.L.); liuyuchuan@mail.dlut.edu.cn (Y.L.); luotong14@mail.dlut.edu.cn (T.L.); liuqingyuan594@mail.dlut.edu.cn (Q.L.); fenglie2021@163.com (L.F.)
[3] Aerospace Information Research Institute, Chinese Academy of Sciences (CAS), Beijing 100094, China; jiaowl@aircas.ac.cn
* Correspondence: liuming@dlut.edu.cn

Abstract: With the continuously growing city size and the increasingly complex and changeable light environment in the city, remote sensing and ground-measured technologies have certain limitations in the research of urban night light environment. The ground-measured data are accurate but low in efficiency and small in scale, while the night-light remote sensing data have the characteristics of high accuracy and large coverage. In this paper, high-resolution night-light remote sensing data and high-accuracy ground-measured data were used to establish an urban ground light environment inversion method with the advantages of remote sensing and ground-measured data in a "space-ground collaboration" approach. A ground database is constructed in GIS based on 26,000 ground measurement data of 4 blocks, 3 spatial perspectives, and 3 light environment parameters. Based on the comparison of the numerical relationship between the measured data of each light environment parameter and each window, the horizontal window is selected as the target window for the ground night light environment inversion research. The urban night light environment inversion method based on the correlation between telemetry and ground- measurement is used to construct and compare the correlation between Luojia night light radiance data and 9 sets of measured data of different ground windows and different light environment parameters. The illuminance measured data of horizontal window and Luojia radiance data, both of which are highly correlated, are selected for regression analysis. The mathematical inversion model of ground illuminance is constructed based on the cubic polynomial model with the lowest RMSE among the six regression models. The inversion result not only has photometric calibration, but also is superior to the original data in terms of population data relevance and accuracy.

Keywords: night light environment inversion; remote sensing observation; ground-measurement

Citation: Zhang, B.; Li, Y.; Liu, M.; Liu, Y.; Luo, T.; Liu, Q.; Feng, L.; Jiao, W. Research on Inversion and Correction Method of Urban Light Environment Based on Cooperative Observation. *Remote Sens.* **2022**, *14*, 2888. https://doi.org/10.3390/rs14122888

Academic Editors: Ahmed Mustafa and Andreas Rienow

Received: 16 May 2022
Accepted: 13 June 2022
Published: 16 June 2022

1. Introduction

With the promotion of urban infrastructure and the development of economy, the number of artificial light sources used for urban night lighting has increased sharply. The rapidly increasing amount of night lighting has had a definite negative impact on the regional ecological environment [1], human health [2], astronomical observation [3], energy consumption [4] and traffic safety [5], and also has formed a complex and changeable urban night light environment. How to use the advanced digital observation technology to provide a comprehensive and systematic monitoring method for the treatment of urban night light environment has become an urgent problem to be solved. In the study of night light environment, there are two main observation methods: one is to collect ground light environment data by field measurement, the other is to obtain night light satellite data source with the help of remote sensing technology.

The emergence of measurement technology is decades earlier than that of remote sensing technology. After a long period, the night light environment research based on measurement has formed a quite systematic research method and produced a large number of research results. For example, Tahar (2017) et al. used the measured data of sky quality meter (SQM) to draw the spatial model of sky brightness on Langkawi Island [6]. Yang Xinxin (2018) used illuminance meter and sky quality meter (SQM) to analyze the urban night artificial light environment in Dalian and Milan [7]. Puching (2020) et al. used the measurement network composed of 23 sky quality meter (SQM) to analyze the periodic changes of urban light environment [8]. Kollath (2020) et al. used CDD camera to study the relationship between color and urban light pollution [9].

In the early study of urban night light environment based on remote sensing, due to the influence of satellite spatial resolution, only large-scale studies such as global and national studies could be implemented. Before the 20th century, most of the studies focused on the large-scale distribution characteristics of light pollution. For example, Butt used DMSP data to estimate the distribution of light pollution in the suburbs of Pakistan [10]; Netzel used VIIRS data to map the distribution of night light environment in Poland [11]. After the 20th century, although the spatial resolution of satellite data had little improvement, the temporal resolution has been improved a lot. During that time, the research focused on the prediction model and growth rate of urban night light environment based on long-time serial night light remote sensing data. Small C, Elvidge and others (2013) used long-time serial data to draw the night light change map of Asian countries from 1992 to 2009 [12]. Jiang Wei (2017) used VIIRS data to analyze the temporal and spatial pattern of night light environment in China [13]. The launch of Luojia high-resolution night light satellite in 2018 has improved the spatial resolution of night light data qualitatively. Some scholars have also carried out some research based on high-resolution data. Guo et al. conducted an on-orbit calibration and an accuracy verification of night light data for Luojia [14]. Hao Qingli used Luojia telemetry data to study the night light environment of the city square [15].

However, as the city size is expanding and the urban space lighting is complex and ever changing, remote sensing and measured technology have certain limitations in the research of urban night light environment [16,17]. The measured technical data is accurate, but it is limited by the number of measuring instruments and the accessibility of the measuring area. Although remote sensing observation technology has the characteristics of large-scale and high-precision, it lacks the commonly used radiation calibration and systematic data processing methods in the field of construction. DMSP and VIIRS data are gray value dot matrix images, and Luojia data are radiance data. Therefore, it is impossible to directly carry out the quantitative study of night light environment with photometric units. Katz believes that there is a statistically significant correlation between the SQM measured data in the upper and horizontal windows and the EROS-B remote sensing data [18] Li, Jiayi used the measured illuminance data and the Luojia night light image with a resolution of 130 m to establish the night radiation correction model of the environment and drew the night light environment map of Nanjing [19]. Liao Zhihong established a regression model based on the measured data of surface temperature and the infrared band data of Landsat TM (30 m resolution) and inverted the surface temperature [20]. Existing studies mostly use a single light environment parameter to carry out research [21]. This paper takes the spatial distribution characteristics of the urban night light environment into consideration, establishes a multi-parameter and multi-spatial perspective ground database, aims to explore the relationship between remote sensing and measured data using correlation analysis, regression models and other methods and to construct a collaborative observation mechanism with the advantages of remote measurement and actual measurement and an inversion method of the urban night light environment. It also explores the actual application scenarios of the inversion results to a certain extent and provide data support for large-scale, high-precision urban night light environment research.

2. Research Method

2.1. Study Area

Dalian is an important central city, port and scenic tourist city in northern China [22]. A unique urban night lighting system has formed. The lights can be lined up and penetrate through the districts in different styles. This paper takes the uniformity of field measurement data sample and the development of various districts and counties in Dalian into consideration when conducting the research on the correlation between remote sensing data and field measurement data. The research focuses on Ganjingzi District, Shahekou District, Zhongshan District, Xigang District, Lushunkou District, and Jinzhou District in Dalian (the diagonal line in Figure 1).

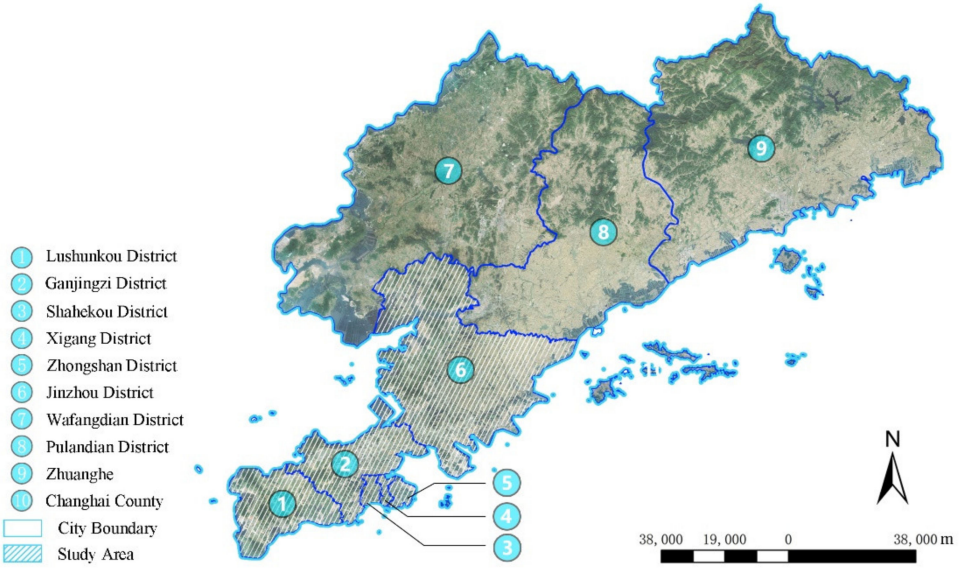

Figure 1. Research areas in Dalian of this paper.

2.2. Research Method

The technical route of this article is shown in Figure 2. First, the Luojia-01 high-precision night light remote sensing data and the measured night light database of multiple-parameter, and multiple-spatial viewing angle perspectives measured night light database are preprocessed. The consistency of geographic location and the consistency of the atmospheric environment are ensured. Subsequently, the correlation analysis between the remote sensing data and the magnitude, brightness, and illuminance data of the three windows (upper, horizontal, and lower windows) is carried out to clarify the relationship between the remote sensing data and the ground light environment parameters. According to the correlation analysis results, the ground light environment parameter has the highest correlation with remote sensing data and is selected as the target inversion parameter. Finally, six commonly used regression models are used to study the mathematical relationship between remote sensing observation data and ground-measured data. The mathematical inversion model of the ground data is established by the mathematical equation with the highest degree of fitting, and the inversion result is verified through the fitting result of the population data of each street and the waveform comparison between the inversion data and the original data.

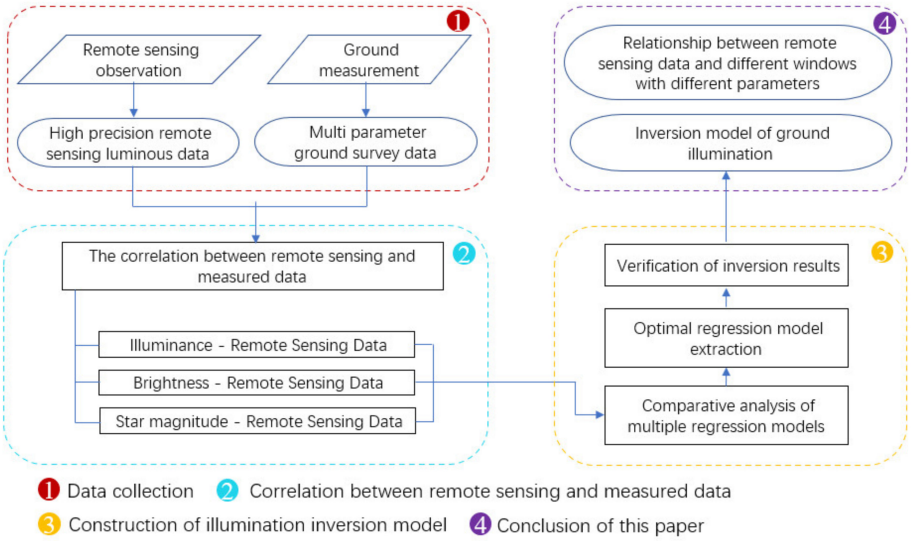

Figure 2. Technical route of this chapter.

2.3. Data Processing

2.3.1. Measured Data Collection and Processing

In order to make the measurement units more evenly arranged in the study area, a total of 249 measurement units are used as the first-level measurement points of the ground measurement data in this paper including the densely distributed 206 measurement units (the red part in the figure) in Chapter 4 Xinghaiwan Street, Heishijiao Street, Qingniwaqiao Street, and Chunliu Street, and 43 measurement units (the blue part in the figure) dispersedly arranged in other research areas of Dalian, and The distribution of each measurement unit in Dalian is shown in Figure 3.

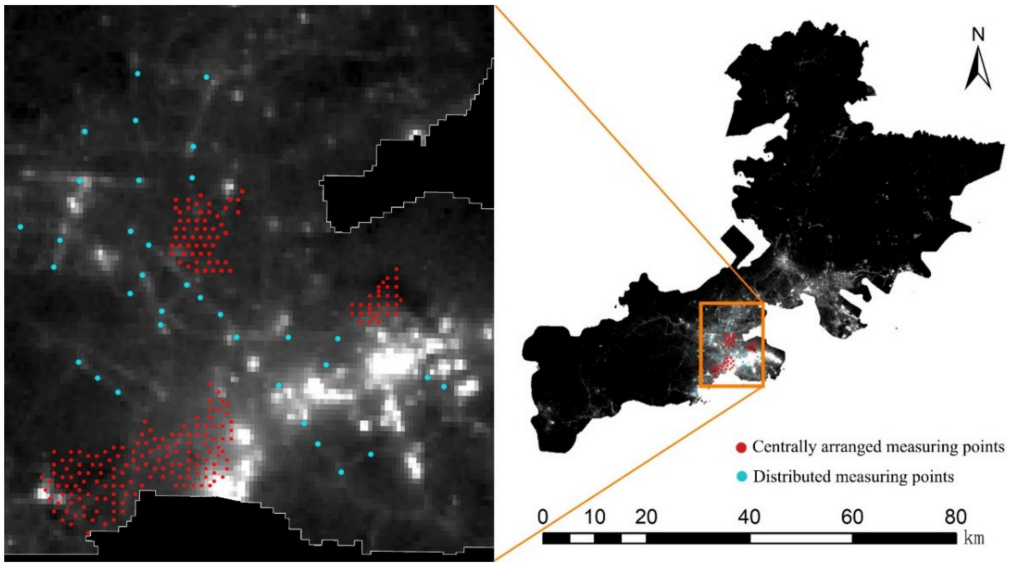

Figure 3. Distribution map of measurement points.

The overall measurement process is shown in Figure 4. In terms of building the measurement unit, the pixel grid of luojia-01 remote sensing image and the GPS coordinates of grid points are extracted to cover the research area. After the research area is covered by pixel grid points, the measuring unit is constructed with the smallest grid size (130 × 130 m). On the division of measurement units, the concept of point density is established, and through the comparative test, it is established that four measurement

points (secondary measurement points) in a grid is the best density for the disassembly measurement of the measured unit.

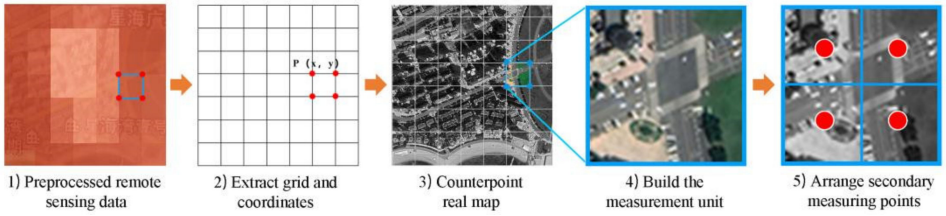

Figure 4. The relationship between remote sensing data and measured data.

Division of measurement windows, three observation windows (upper, horizontal, and lower windows) divide the ground space into three directions (Figure 5) at each secondary measurement point. The upper window mainly observes the light environment of the night sky layer of the city. The horizontal window mainly observes the light environment of the human eye in the horizontal direction. The lower window mainly observes the light environment on the ground.

Figure 5. Measurement method of ground windows.

Measurement process of each measuring point: Four night-time urban light environment parameters of illuminance, magnitude brightness, brightness, and spectrum are measured in each window. The horizontal surrounding measurement is conducted at 45-degree intervals in the horizontal direction. The upper and lower windows are measured parallel to the ground for a single direction. The instruments used in each direction are shown in Figure 6.

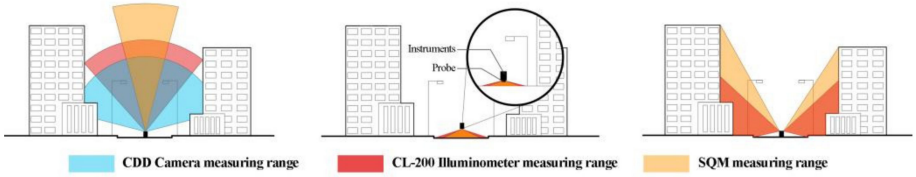

Figure 6. Types of observation instruments used in each window.

After obtaining the measurement data, it needs to be processed. The data processing method is as follows: calculate the average value of the eight directions of the horizontal window of each secondary measuring point to obtain the horizontal direction data of each secondary measuring point. Then, the horizontal direction data of four secondary measuring points in one measuring unit are averaged again to obtain the illuminance data in the horizontal direction of the measuring unit. The illuminance data of upper windows and lower windows in the measuring unit is also calculated in the method above.

2.3.2. Remote Sensing Data Processing

This article uses the Luojia-01 night light remote sensing open-source data from Hubei Data and Application Network [23] (http://www.hbeos.org.cn, accessed on 1 August 2019) We download Luojia-01's 10 night lighting images on 17 March 2019, 9 March 2019,

9 September 2018, 5 September 2018, and 28 August 2018 [24]. Raster calculator tool in GIS (Geographic Information System) is used to perform noise reduction, geographic correction, and radiation value conversion processing on 10-night light data to obtain the Dalian Luojia-01 luminous remote sensing data set after preliminary processing [25]. As shown in Figure 7.

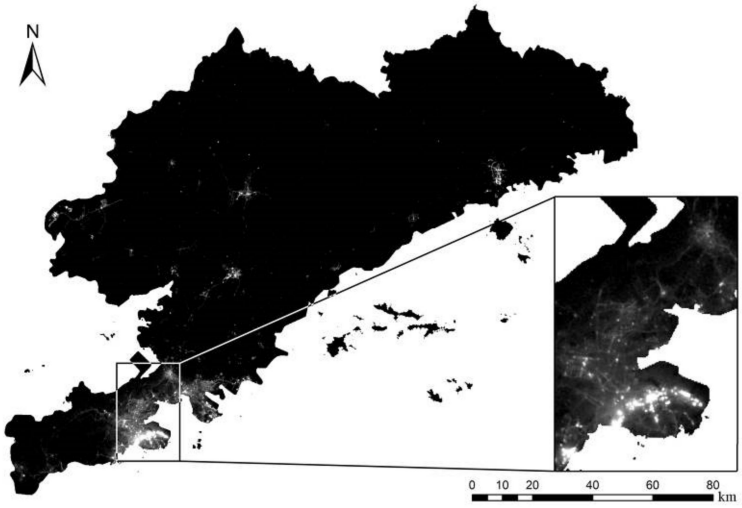

Figure 7. Preprocessed remote sensing data of night light in Dalian.

2.4. Model Construction

This paper discusses the mathematical relationship between the measured ground illuminance data and the telemetry radiance data in the study of light environment [19], and establishes the inversion model of ground illuminance based on the mathematical relationship between the data. The three specific methods are as follows:

Firstly, the ground light environment measured data of three spatial windows (upper, horizontal and lower) and three light environment parameters (magnitude brightness, brightness and illuminance) after preprocessing are used to analyze the correlation with the radiation brightness data of Luojia Dalian. Through the comparison of correlation parameters, the relationship between remote sensing observation data and parameters of different ground light environment and different spatial perspectives is clarified, so that the target inversion parameters are extracted and provide the basis for the selection of light environment parameters and spatial windows for the ground light environment inversion model associated with telemetry and measurement. Secondly, the construction and comparison of the model is conducted as follows: the stratified sampling process is added to the traditional standard K-fold cross-validation method, which is used to sample the original data set, so as to ensure that the numerical distribution of the samples in the correction set and validation set maintains the same proportional characteristics as that of the original data set, and reduce errors. In order to obtain a reliable mathematical model, six regression models are used: univariate linear model, quadratic polynomial model, cubic polynomial model, exponential model, logarithmic model and power function model. Finally, the inversion results are verified by population data and data waveform.

3. Result

3.1. Measured Data Processing Results

The measured data of three windows and three light environment parameters of 960 secondary measuring points are processed by the above method. A total of 38,000 light environment measurement data of secondary measuring points is processed, and 240 measurement units' data sets of three windows and three light environment parameters are obtained.

The comparison of the illuminance maps of the three windows in 4 regions shows that, from the perspective of spatial distribution characteristics, the high-value raster pixel points of the three windows correspond to business and commerce, and the low-value points are parks, urban squaresand residential area. For example, in the horizontal window of Heishijiao Street (Figure 8h), the high-value raster pixels in the window are mostly distributed on both sides of the urban main road and the urban commercial area on both sides of the Heishijiao subway station. The low-value raster pixels in the window are mostly distributed in the Xijianshan Park on the north side of the window, the Wencuixuan community on the west side and the Xigou residential community on the west side. In the window (Figure 8a) on Xinghaiwan Street, high-value raster pixels are located in the Convention and Exhibition Center and Futures Building on the east side of the study area. Raster pixels with lower values are mostly distributed in Phu Quoc Park on the north side of the street and the surrounding old communities.

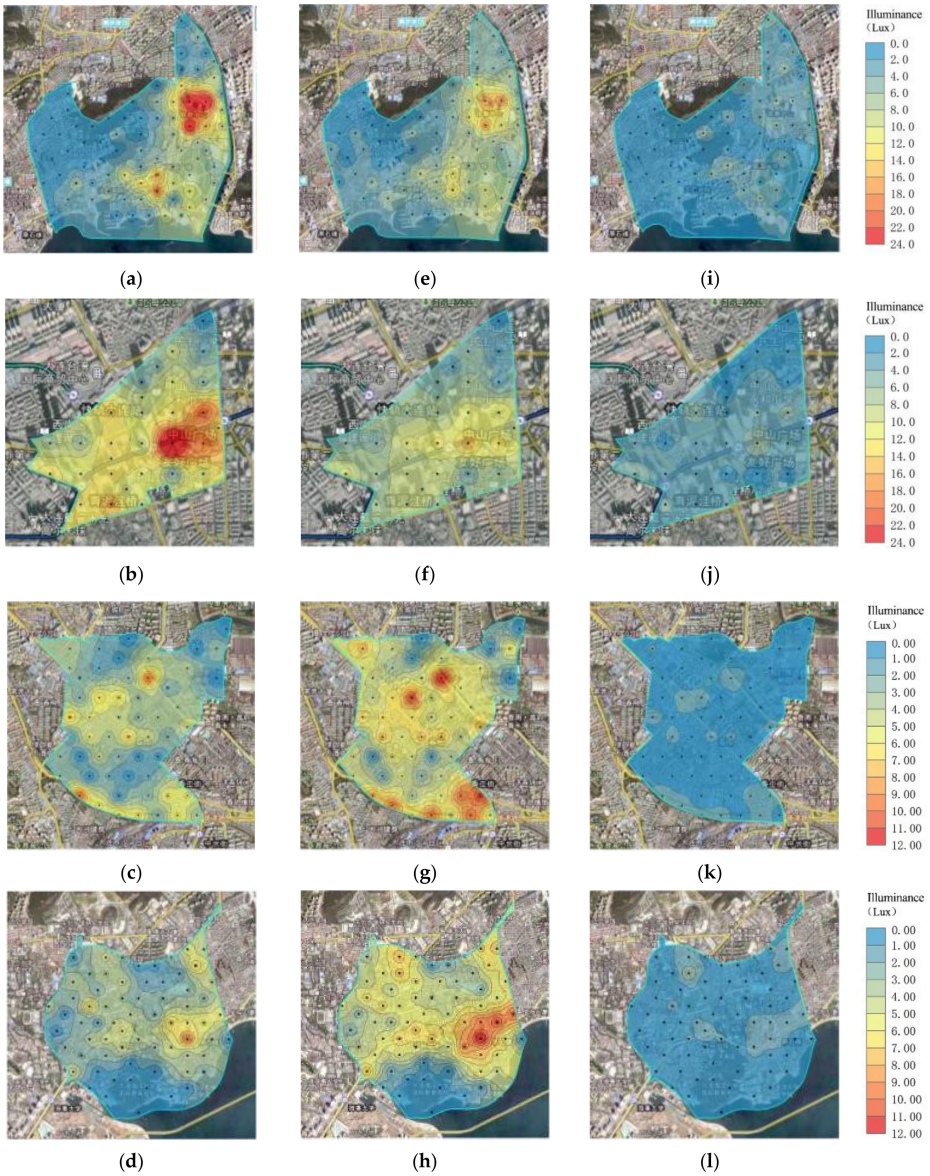

Figure 8. Illumination distribution in three directions of high value area. (**a**) Xinghaiwan upper window; (**b**) Qingniwa upper window; (**c**) Chunliu upper window; (**d**) Heishijiao upper window; (**e**) Xinghaiwan horizontal window; (**f**) Qingniwa horizontal window; (**g**) Chunliu horizontal window; (**h**) Heishijiao horizontal window; (**i**) Xinghaiwan lower window; (**j**) Qingniwa lower window; (**k**) Chunliu lower window; (**l**) Heishijiao lower window.

From the point of view of the difference of values between different windows, the illuminance value of the upper window is slightly larger than that of the horizontal window, but the illuminance values of the upper window and the horizontal window are much larger than that of lower window. Among that, the illuminance values of 71.3% and 90.59% of the horizontal window area of Xinghaiwan (Figure 8e) and Qingniwa Bridge (Figure 8f) are more than twice that of the lower window area of the two administrative division, respectively (Figure 8i,j). In addition, 74.3% of the horizontal view windows of Chunliu Street (Figure 8g) and 81.9% of the horizontal view windows of Heishijiao Street (Figure 8h) have illuminance values that are more than twice the highest value of the corresponding lower windows (Figure 8k,l).

The comparison of the brightness maps of the three windows in 4 areas shows that from the perspective of spatial distribution characteristics, the three windows have a certain similarity. The high-value raster pixel points in the three windows are all distributed around urban arterial roads and commercial office buildings. The low-value raster pixel points are distributed around residential areas and parks. For example, in e Heishijiao Street horizontal window (Figure 9h), the high-value raster pixels in the window are concentrated around the commercial area of Heishijiao on the east side. The low-value raster pixels are mostly distributed in Dongbei University of Finance and Economics and the coastal area of the city to the north. In Xinghaiwan Street lower window (Figure 9i), the high-value raster pixels are mostly distributed in the urban commercial cluster formed by Convention and Exhibition Center, Dalian Futures Building, and Grand Hyatt Hotel. Some high-value raster pixels are distributed on the in the commercial clusters on east side of Xinghai Square and around Dalian Mingzhu District.

Numerically, the brightness values of the horizontal window are much greater than that of the upper and lower windows. The brightness values of the horizontal window area of 71.3%, 90.59%, 82.3%, and 92.16% of Xinghaiwan Street (Figure 9e), Qingniwa Bridge (Figure 9f), Heishijiao (Figure 9g), and Chunliu Street (Figure 9h) are more than twice the brightness values on each street.

The comparison of the magnitude brightness maps of the three windows in the two regions shows that, in terms of the relationship between the magnitude brightness and urban functions, the three windows have certain consistency. The corresponding city functions of high-value raster pixel points are squares, coasts, parks, and residential areas, and that of low-value raster pixel points are business districts, office areas, urban roads, and urban square areas. For example, in the upper window on Xinghaiwan Street (Figure 10a), the high-value points are mostly distributed in Phu Quoc Park and surrounding residential areas. The low-value points are mostly distributed on the main urban roads and around the exhibition center. In the Chunliu upper window (Figure 10c), the high-value points are mostly distributed around the Dalian Shipyard and the new communities. The low-value points are mostly distributed around Xiangzhou Road and Wuzhou Building.

The values of the windows show certain consistency of the four streets. The magnitude brightness value of more than 70% of the horizontal window area is between 10–13 mag/arcsec^2, which is 4–5 mag/arcsec^2 smaller than the upper and lower windows, respectively.

(**a**) (**e**) (**i**)

Figure 9. *Cont.*

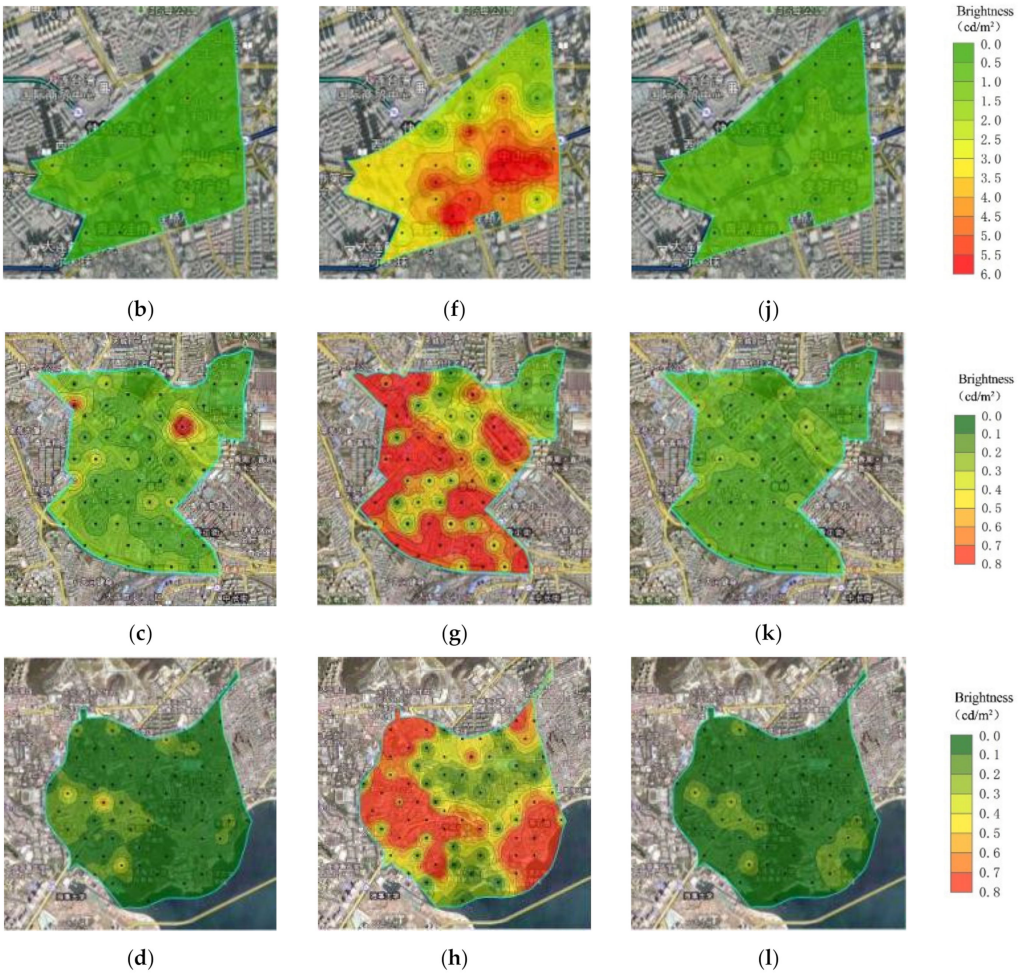

Figure 9. Brightness distribution in three directions of high value area. (**a**) Xinghaiwan upper window; (**b**) Qingniwa upper window; (**c**) Chunliu upper window; (**d**) Heishijiao upper window; (**e**) Xinghaiwan horizontal window; (**f**) Qingniwa horizontal window; (**g**) Chunliu horizontal window; (**h**) Heishijiao horizontal window; (**i**) Xinghaiwan lower window; (**j**) Qingniwa lower window; (**k**) Chunliu lower window; (**l**) Heishijiao lower window.

3.2. Inversion Model

3.2.1. Target Inversion Parameter Extraction

Through the comparison of the Pearson correlation coefficients and R^2 values of the three windows, we found that the illuminance value distribution of the upper window, the horizontal window, and the lower window all have a significant positive relationship with the Luojia-01 remote sensing observation results. However, the correlation results of the upper window and the horizontal window are better than those of the lower window. Therefore, for the illuminance parameters, the Luojia-01 remote sensing data has a better illustration to the ground illuminance data of the upper and horizontal windows.

As we take the observed values of the magnitude brightness in each window as the independent variable, and the Luojia radiance data as the dependent variable, the R^2 of the regression analysis of the upper window (Figure 11d) is 0.181; the Pearson correlation coefficient of the two is -0.425 ($p = 0.000 < 0.01$), the R^2 of the regression analysis in the horizontal window (Figure 11e) is 0.272; the Pearson correlation coefficient is -0.522 ($p = 0.000 < 0.01$), and the R^2 of the regression analysis in the lower window (Figure 11f) is 0.183; the Pearson correlation coefficient is -0.428 ($p = 0.000 < 0.01$). The correlation index between the horizontal window magnitude data and Luojia data is better than that of the lower window and the upper window. Therefore, in terms of magnitude parameters, Luojia radiance data can better reflect the distribution of ground level windows.

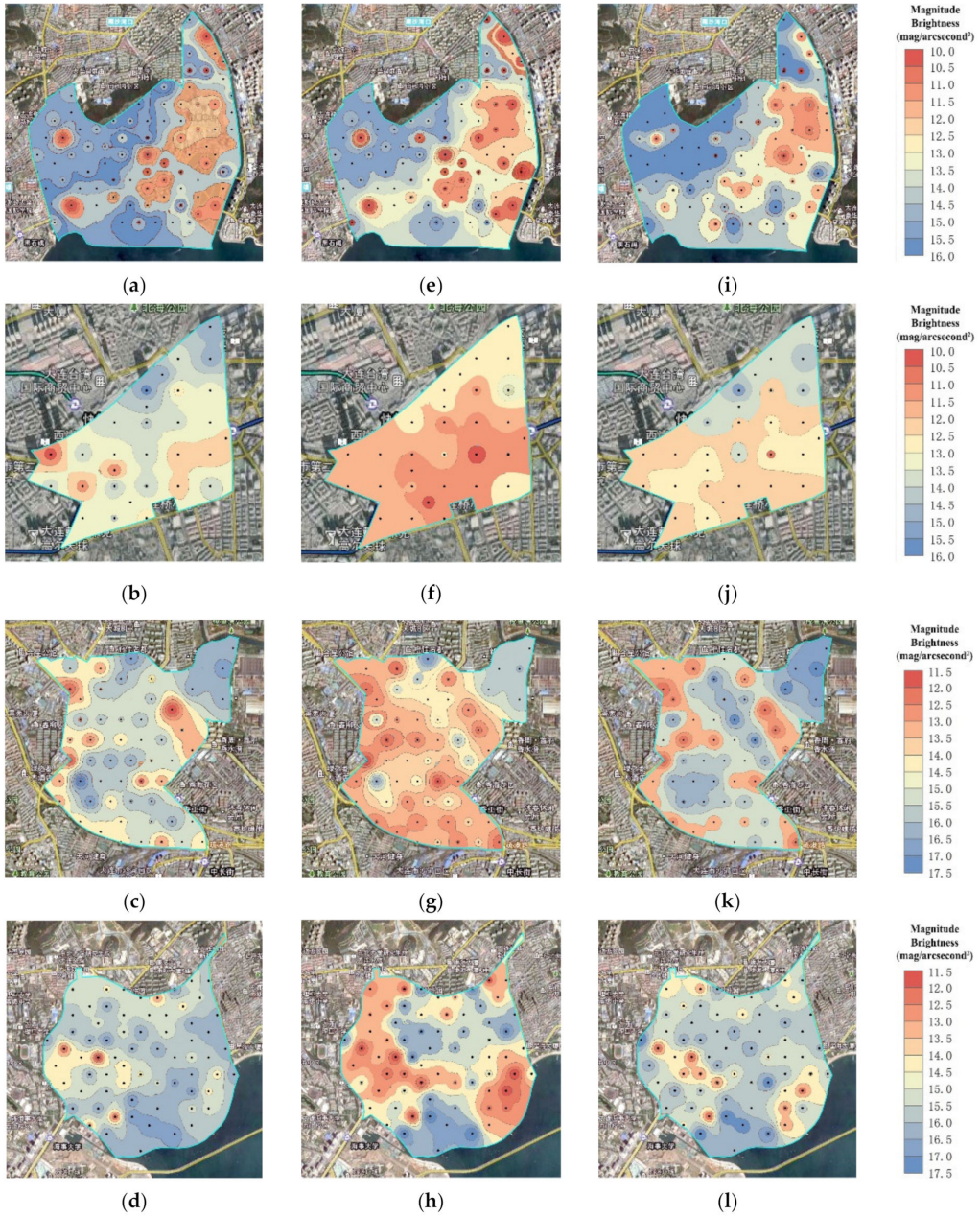

Figure 10. Magnitude brightness distribution in three directions of high value area. (**a**) Xinghaiwan upper window; (**b**) Qingniwa upper window; (**c**) Chunliu upper window; (**d**) Heishijiao upper window; (**e**) Xinghaiwan horizontal window; (**f**) Qingniwa horizontal window; (**g**) Chunliu horizontal window; (**h**) Heishijiao horizontal window; (**i**) Xinghaiwan lower window; (**j**) Qingniwa lower window; (**k**) Chunliu lower window; (**l**) Heishijiao lower window.

As the illuminance observations in each window are used as independent variables, and Luojia radiance data is the dependent variable, the R^2 of the regression analysis of the upper window (Figure 11a) is 0.805; the Pearson correlation coefficient is 0.897 ($p = 0.000 < 0.01$), and the horizontal window (Figure 11b) R^2 of regression analysis is 0.760; Pearson's correlation coefficient is 0.872 ($p = 0.000 < 0.01$), but the correlation index between the upper window and the horizontal window and Luojia radiance data is better than that of the lower window, so in terms of the illuminance parameter, Luojia data has a more accurate reflection of the numerical distribution of the illuminance of upper windows and horizontal windows on the ground.

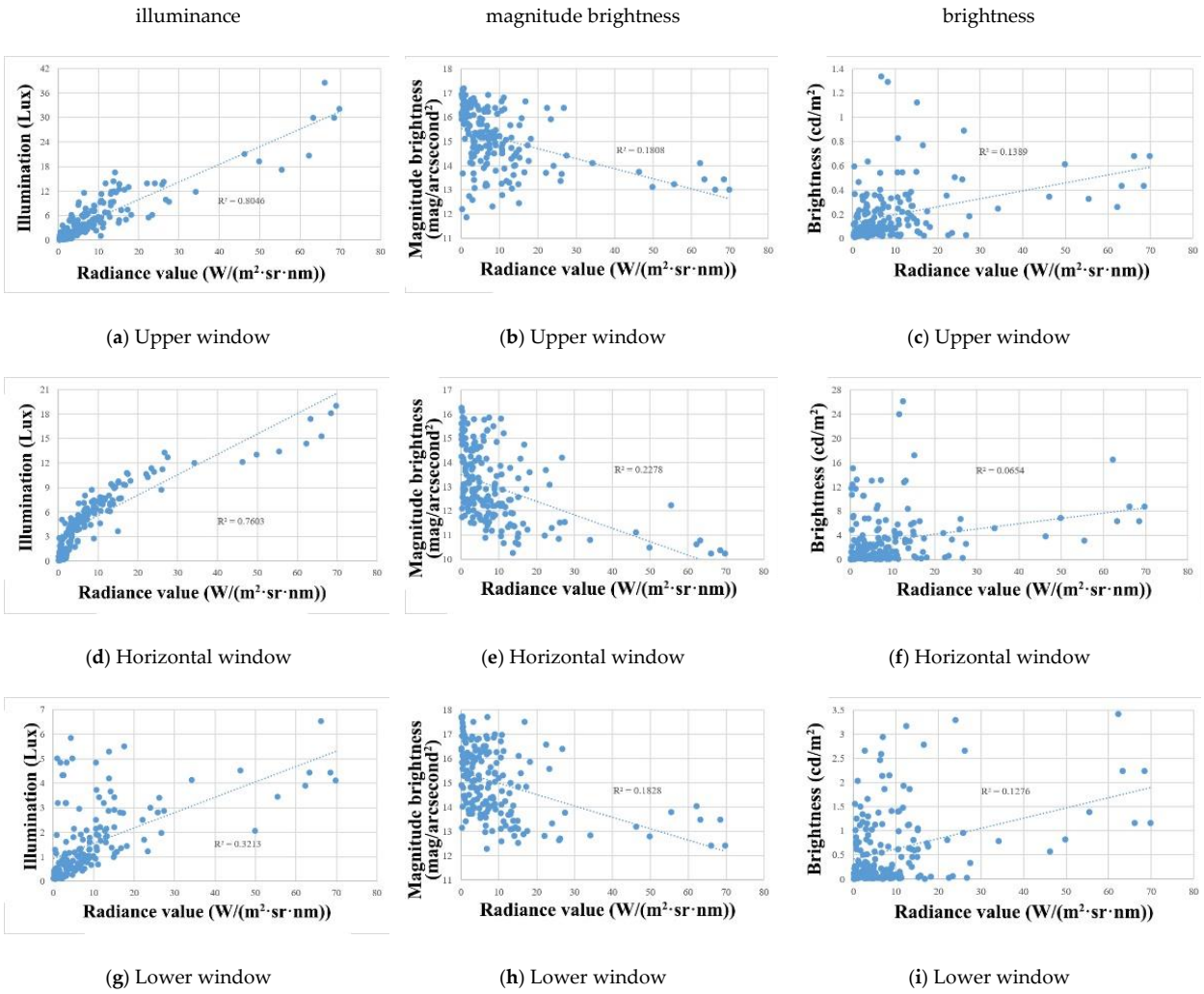

(**a**) Upper window (**b**) Upper window (**c**) Upper window

(**d**) Horizontal window (**e**) Horizontal window (**f**) Horizontal window

(**g**) Lower window (**h**) Lower window (**i**) Lower window

Figure 11. Fitting diagram of measured data and remote sensing data of illuminance of each window.

As the observed values of brightness in each window are used as independent variables, Luojia radiance data as the dependent variable, the R^2 of the regression analysis of the upper window (Figure 11g) is 0.218; the Pearson correlation coefficient is 0.467 ($p = 0.000 < 0.01$), and the horizontal window (Figure 11h) The regression analysis R^2 is 0.454; the Pearson correlation coefficient is 0.647 ($p = 0.000 < 0.01$), the lower window (Figure 11i) the regression analysis R^2 is 0.128; the Pearson correlation coefficient is 0.353 ($p = 0.000 < 0.01$), Therefore, the correlation index of the upper window, the horizontal window and the remote sensing data is better than the lower window. Therefore, in terms of the brightness parameters, Luojia radiance data reflects the distribution of windows and horizontal windows on the ground more accurately.

The study of the spatial distribution characteristics of the ground nighttime light environment in Section 3.1 found that the horizontal viewport is the high-value viewport for artificial illumination at night. In addition, the telemetry radiance data of Luojia can have a good correlation with the horizontal and upper windows of the illuminance parameters in the ground light environment parameters (Table 1). Therefore, the illuminance data of the horizontal window is used as the inversion target, and the mathematical regression relationship between the measured illuminance data of the horizontal window and the Luojia telemetry radiance data is used to establish the inversion model of the illuminance of the horizontal window on the ground.

Table 1. Pearson analysis of illuminance data and remote sensing data.

Window	Parameter	Luojia-01 Correlation Analysis of Remote Sensing Data	
		The Correlation Coefficient of Pearson	*p* Value
Illuminance	Upper Window	0.897 **	0.000
	Horizontal Window	0.872 **	0.000
	Lower Window	0.567 **	0.000
Magnitude of brightness	Upper Window	−0.425 **	0.000
	Horizontal Window	−0.477 **	0.000
	Lower Window	−0.428 **	0.000
Brightness	Upper Window	0.373 **	0.000
	Horizontal Window	0.256 **	0.001
	Lower Window	0.357 **	0.000

** indicates a 1% significance level (two-tailed), ($p = 0.000 < 0.01$).

3.2.2. Model Construction and Comparison

Data Packet

In this study, stratified K-fold cross-validation method (Figure 12) are used to conduct stratified sampling of 167 sets of original data sets from remote sensing and field measurement [26]. The original data are divided into four data groups: A, B, C and D, and the numerical distribution characteristics of each group are the same as the original data sets. The four data sets are divided into four combinations according to the combinations of different correction sets and verification sets. The correction set and verification set of each combination are shown in Table 2.

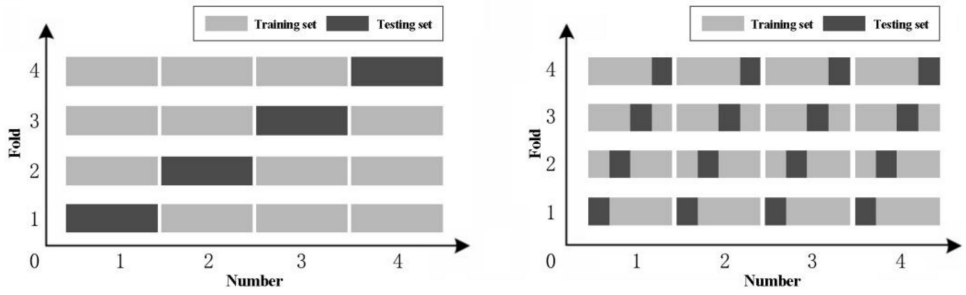

(**a**) (**b**)

Figure 12. Hierarchical k-fold cross validation data grouping diagram. (**a**) Standard K-fold cross validation; (**b**) Stratified K-fold cross validation.

Table 2. The combination results of different correction sets and verification sets.

Combination Name	Correction Set	Validation Set
Combination 1	Group A, Group B, Group C	Group D
Combination 2	Group A, Group C, Group D	Group B
Combination 3	Group A, Group B, Group D	Group C
Combination 4	Group B, Group C, Group D	Group A

Model Contrast

Six regression models are used in this study, including unitary variable linear model, quadratic polynomial model, cubic polynomial model, exponential model, logarithmic model and power function model. Based on the data grouping in the stratified K-fold cross-validation method, four iterative regressions are carried out for each regression model according to the number of data groups. In each time of regression, three groups of data are taken as the correction set, and the remaining one is taken as the validation set. In each

regression, the correction set is used to build a regression model, and the satellite remote sensing data in the verification set is used to simulate the ground illuminance data, and the root mean square error (RMSE) and R^2 mean value of the simulated value and the actual value in the verification set were calculated to evaluate the accuracy of inversion results.

In the regression analysis of the power function model (Figure 13a), from the image, the curves of regression models of different combinations have certain consistency. The R^2 values of data combination 1–4 were similar, which were 0.713, 0.699, 0.701 and 0.704, respectively.

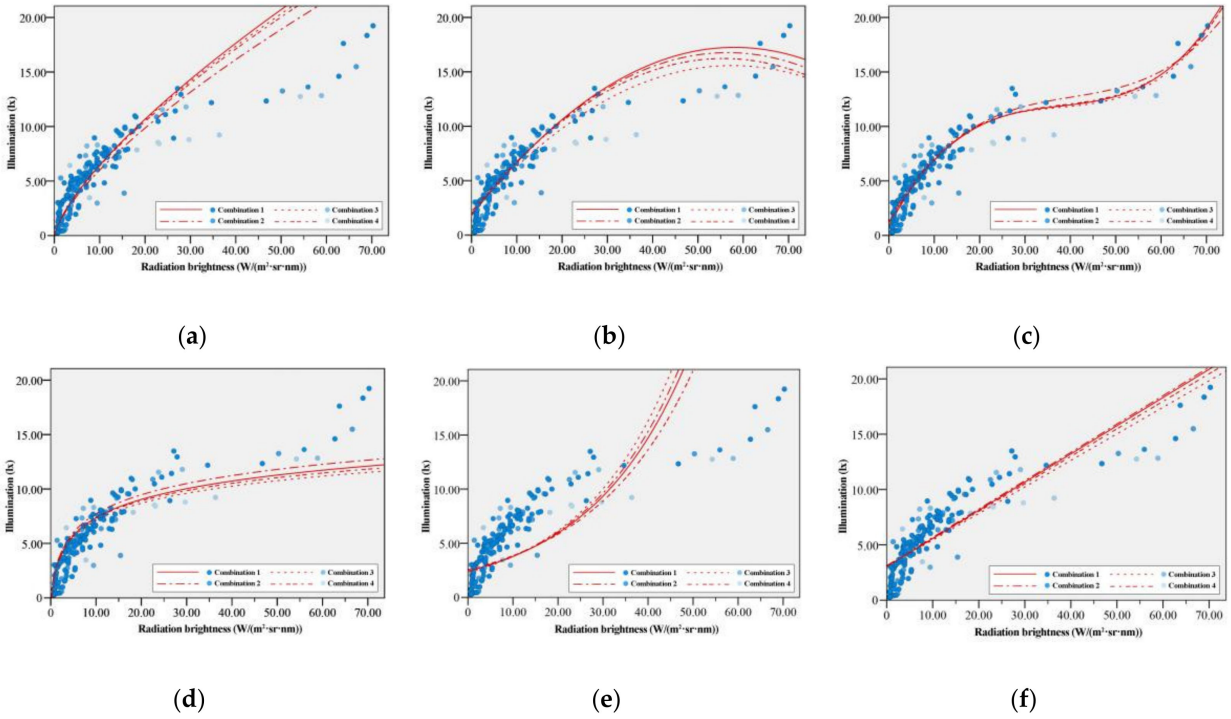

Figure 13. Exponential function regression graph of each modified set. (**a**) Power function; (**b**) Quadratic function; (**c**) Cubic function; (**d**) Logarithmic function; (**e**) Exponential function; (**f**) Linear function function.

In the regression analysis of the quadratic polynomial model, from the image (Figure 13b), the curves of the regression model of different data combinations fit well. R^2 of data combination 1–4 were 0.884, 0.872, 0.819 and 0.851, respectively. Except for combination 3, the R^2 values of all data combinations have little difference. In the regression analysis of the cubic polynomial model, from the image (Figure 13c), the curves of the regression model with different data combinations fit well. R^2 of data combination 1–4 were 0.909, 0.891, 0.899 and 0.895, respectively. R^2 value of each data combination ranges from 0.89 to 0.91.

In the regression analysis of the logarithmic function model, from the image (Figure 13d), the curves of the regression model with different data combinations fit well. The R^2 values of all data combinations were similar, and the R^2 values of data combinations 1–4 were 0.770, 0.769, 0.767, and 0.755, respectively.

Exponential function (Figure 13e) and linear function regression model (Figure 13f) analysis are as follows. In the exponential function regression model, the R^2 of the fitting results of each combination is too low, while the unary linear function uniformly assigns a value of 3.8 lx for the illuminance value lower than 3.8 lx, and the fitted curve and the scattered points do not fit. The generated functional model has no explanatory significance for the sample distribution.

The regression results of each group of correction sets in the four groups of data are used to establish mathematical models, respectively, and the ground illuminance data of each group of verification sets are inverted and estimated by each group of mathematical models, respectively. A line chart comparing the estimated value of illuminance inversion with the measured value of illuminance is drawn. (Figure 14).

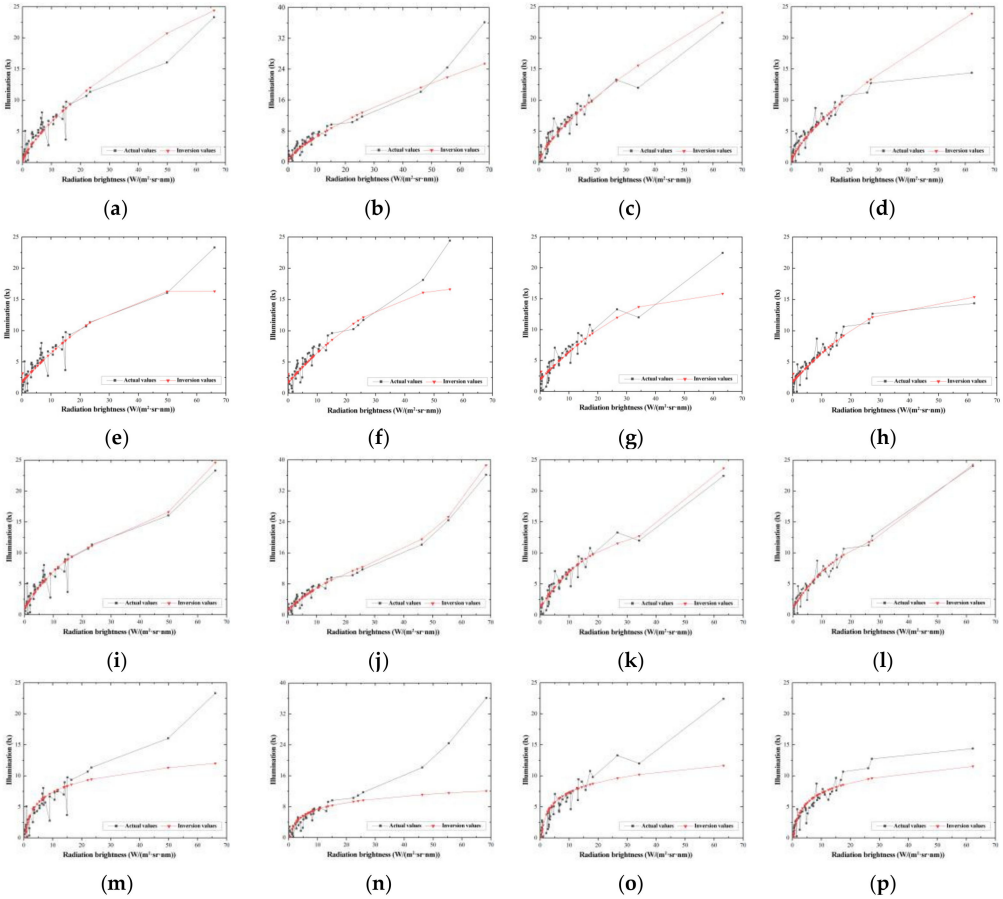

Figure 14. Comparison of actual value and inversion estimation of illuminance of each group. (**a**) Power functions-combination 1; (**b**) Power functions-combination 2; (**c**) Power functions-combination 3; (**d**) Power functions-combination 4; (**e**) Quadratic functions-combination 1; (**f**) Quadratic functions-combinations 2; (**g**) Quadratic function-combination 3; (**h**) Quadratic func-tions- combination 4; (**i**) Cubic functions-combination 1; (**j**) Cubic functions-combination 2; (**k**) Cubic functions-combination 3; (**l**) Cubic functions-combination 4; (**m**) Log functions-combination 1; (**n**) Log functions-combination 2; (**o**) Log functions-combination 3; (**p**) Log functions-combination 4.

For the power function model (Figure 14a–d), in the range of 0.0–10.0 lx illuminance, the inversion estimated value of illuminance is in good agreement with the actual value of illuminance, and the illuminance value above 10.0lx will be overestimated. Therefore, it is considered that the power function model has a relatively accurate inversion ability only for the illuminance value between 0.0 and 10.0 lx.

For the quadratic function model (Figure 14e–h), in the range of 2.4–12.0 lx illuminance, the estimated value of illuminance inversion and the actual value of illuminance fit well. However, the model underestimates the illuminance values above 15.0 lx, overestimates the illuminance values within 12.7–15.0 lx, and sets all illuminance values below 2.4 lx as fixed values. Therefore, it is considered that the quadratic polynomial model has a more accurate inversion ability for the ground illuminance value within the range of 2.4–12.7 lx.

For the cubic function model (Figure 14i–l), in the range of 0.0–22.0 lx illuminance, the inversion illuminance value fits well with the actual illuminance value. The overestimation and underestimation of illuminance appears fewer than the other five regression models. Therefore, it is considered that the cubic polynomial model has a relatively accurate inversion ability for the ground illuminance values within the range of 0.0–22.0 lx.

For the exponential function model (Figure 14m–p), in the range of 0.0–9.0 lx illuminance, the inversion estimated value of illuminance is in good agreement with the actual value of illuminance, but the data larger than 9.0 lx is obviously underestimated. Therefore,

it is considered that the logarithmic regression model has a relatively accurate inversion ability for the ground illuminance value within the range of 0.0–9.0 lx. It does not have the ability to invert the illuminance value above 9.0 lx.

The root mean square error (RMSE) values of each combination validation set in the power function, quadratic polynomial, cubic polynomial and logarithmic function regression models were statistically analyzed (Table 3) to evaluate the accuracy of the four regression models applied in ground optical environment inversion.

Table 3. Statistical table of error terms in inversion results of each regression model.

Check the Numerical	Type of Regression Model	Combination 1	Combination 2	Combination 3	Combination 4
Power function	RMSE	1.69	1.99	1.23	1.08
	MRE	59.71	66.53	49.81	65.50
Quadratic polynomial	RMSE	1.77	3.41	1.55	1.67
	MRE	144.72	217.20	101.60	159.38
Cubic polynomial	RMSE	1.17	1.09	1.11	1.00
	MRE	100.23	161.06	76.95	115.15
Logarithmic function	RMSE	2.47	4.49	2.23	2.32
	MRE	241.89	379.94	70.36	117.17

In the power function model, the RMSE values between the four groups of estimated illuminance inversion and the actual illuminance value ranges from 1.08 lx to 1.91 lx, among which the RMSE value of combination 3 is as high as 1.99 lx, which is caused by the power function model's underestimation of the illuminance inversion of multiple ground points above 10 lx in this combination.

In the quadratic function model, RMSE and MRE values of each combination are shown in Table 3. Except for combination 2, the RMSE range between the inversion value and the actual value of the other groups is 1.55–1.77 lx, among which the RMSE value of combination 2 is as high as 3.41lx, which is caused by the deviation of the inversion value of illuminance of several ground points above 12.7 by quadratic polynomial model in this combination.

RMSE and MRE values of each combination in cubic function model are shown in Table 3, the RMSE value range between the inversion value and the actual illuminance value of each combination is 1.00–1.17 lx, among which the RMSE value of combination 4 is only 1.00 lx, and the R^2 value between the inversion estimated value and the actual illuminance value are all greater than 0.90.

RMSE and MRE values of each combination in the exponential function model, are shown in Table 3. Except for combination 2, the RMSE range between the inversion value of illuminance and the actual value of illuminance in other groups is 2.23 to 2.48 lx, among which the RMSE value of combination 2 is as high as 4.49lx, which is caused by the fact that the logarithmic model underestimates the inversion value of illuminance of many ground points above 9.0lx in this combination, making them lower than the actual value.

Among the four regression models, the RMSE value range of the four validation sets of the cubic polynomial regression model is 1.00–1.17 lx, whose error value is the smallest among the four regression models. Logarithmic function regression model has the highest error value, RMSE value range is 2.23–4.49 lx. The inversion accuracy of the four regression models is ranked as: cubic polynomial > power function > quadratic polynomial > logarithmic function.

In addition, neuronal network models are replacing traditional linear and nonlinear regression analysis in recent studies [27]. The two main functions of neural networks are pattern recognition and data fitting. The good nonlinear performance of neural networks can well portray various nonlinear surfaces and thus bring good pattern recognition, while their excellent optimization computational process can solve various function fitting problems, which provides new possibilities for regression analysis.

To sum up, the cubic polynomial model is taken as the mathematical inversion model of Dalian's ground horizontal illuminance, and the model equation is as follows:

$$E = 0.0002L^3 - 0.0182L^2 + 0.7488L + 1.0985 \quad (1)$$

wherein: E is the inversion value of ground horizontal illuminance, lx is the unit; L is the radiation brightness value of Luojia-01 night light data, and the unit is $W/(m^2 \cdot sr \cdot nm)$.

In ENVI, the preprocessed Luojia-01 night-light remote sensing data of Dalian is taken as the input data source, and the bandmath is used to enter the above regression equation (Equation (1)) to carry out the inversion calculation of the ground horizontal illuminance value. The calculated raster image is outputted, as shown in Figure 15.

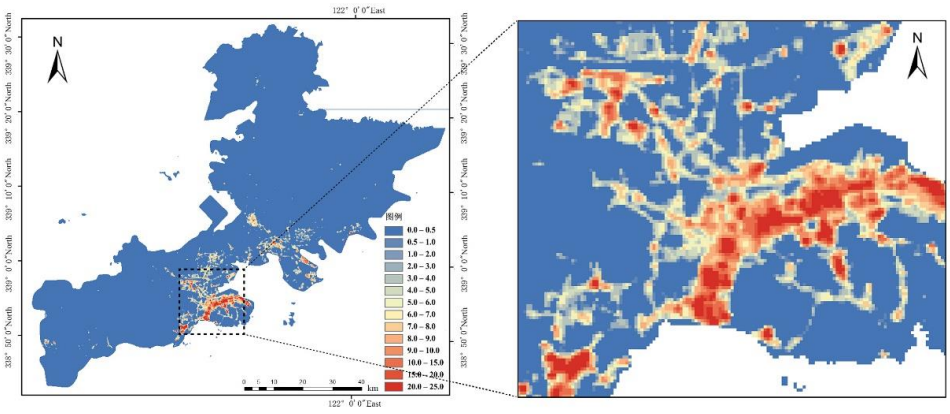

Figure 15. Inversion results of ground horizontal illuminance in main urban area of Dalian City.

3.2.3. Model Validation

Verification of Population Data

In order to evaluate the accuracy of the ground illuminance inversion data, taking the population density data of each street in Dalian as a scale [28], the correlation analysis between the population density data of each street and Luojia-01 night-light remote sensing data of each street, Dalian ground illuminance inversion data is carried out, respectively, as shown in Table 4. The correlation coefficient between illuminance inversion data and population data is 0.714, which is 0.088 higher than the Luojia-01 data.

Table 4. Person correlation analysis of total population, radiance and total retrieved illuminance in each street.

Name	Related Parameters	Total Population	Total Radiant Brightness $W/(m^2 \cdot sr \cdot nm)$	Total Inversion Illuminance (lx)
Total population	Correlation coefficient	1	0.626 **	0.714 **
	p value (double-tailed)		0.000	0.000
Total radiant brightness	Correlation coefficient	0.626 **	1	0.945**
	p value (double-tailed)	0.000		0.00
Inversion of the total illuminance	Correlation coefficient	0.714 **	0.945 **	1
	p value (double-tailed)	0.000	0.000	
	Number of samples	72	72	72

** indicates a 1% significance level (two-tailed); ($p = 0.000 < 0.01$).

It can be seen from Figure 16 that all the inversion illuminance data is relatively continuous and the dispersion degree of the scattered points is low. In terms of R^2 value, the R^2 value of the inversion illuminance value is higher. Compared with Luojia-01 night light data, the inversion results of the ground horizontal illuminance inversion model have a certain improvement in the accuracy of reflecting the ground light environment.

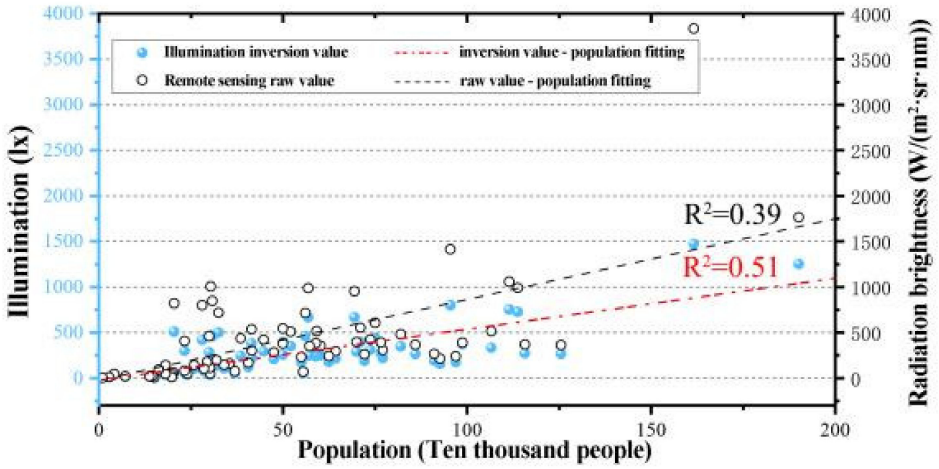

Figure 16. Scatter plot of total population, total radiance and total inversion illuminance of each street.

Ground Data Processing Results

In order to clarify the improvement of illuminance inversion data relative to remote sensing data, two latitude lines are selected in the urban area of Dalian City, and the positions of the two value lines are shown in Figure 17. The geospatial coordinates of the latitude line are used to extract the illuminance inversion data of Dalian Luojia-01 and Dalian City, respectively, and to analyze the advantages of the inversion data by comparing the inversion data of the two value lines at the same position with the waveform diagrams of Luojia data (Figure 18).

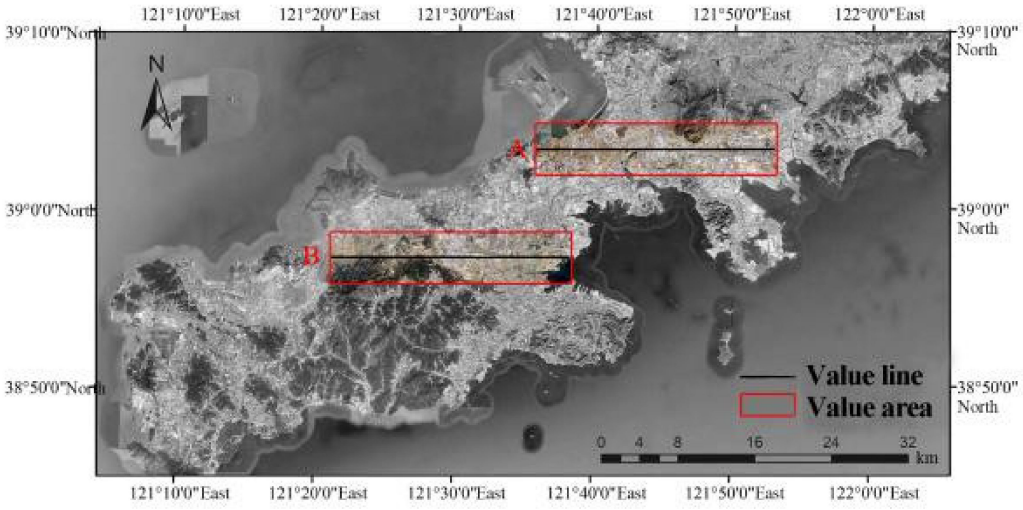

Figure 17. Location diagram of value line.

The value line of region A spans the urban edge area of Dalian Ganjingzi District, and the numerical interval of illuminance inversion value is 0–8 lx (Figure 18a). After comparison, it is found that the inversion model correct well the light supersaturation effect in the high illuminance region of the original remote sensing data, which makes the inversion data continuous numerically.

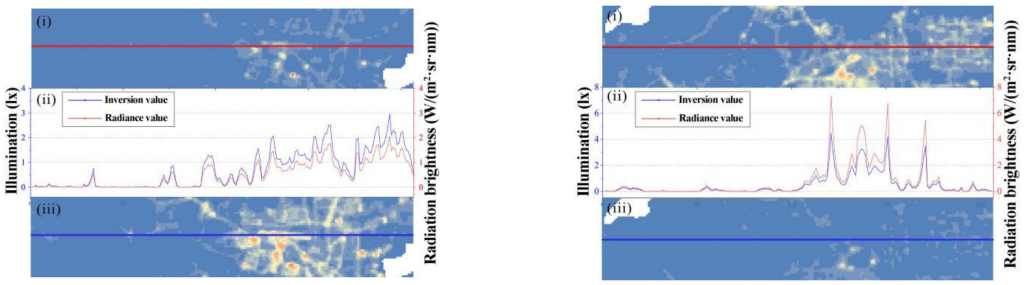

(**a**) (**b**)

Figure 18. Comparison of illuminance inversion data and luojia-01 data. (**a**) Value region A; (**b**) Value region B; (**i**) Luojia-01 remote sensing data; (**ii**) Compare the line chart; (**iii**) Illuminance inversion data.

The value line of region B is across the urban edge area of Jinzhou District, and the numerical interval of illuminance inversion value is 0–2 lx (Figure 18b). Compared with the original remote sensing image, it is found that the inversion model can enlarge the value of the low-illuminance area to some extent, so that the inversion value of the low-illuminance area has a better numerical gradient than the original remote sensing image.

4. Discussion

4.1. Safety Map

Urban night light environment has a direct impact on crime rate and safety [29,30]. Improving the safety in urban night light environment is of positive significance for enhancing the vitality of the city at night. The 130 m resolution urban illuminance inversion data obtained by the ground light environment inversion model in this paper can provide good data support for large-scale lighting safety risk analysis and accurate positioning of risk points, and build the application scenario of illuminance inversion results in urban night light environment governance.

It can be seen from the land classification map of Dalian City (Figure 19) that there are a large number of undeveloped lands such as mountains and beaches in the urban area of Dalian City. Therefore, it is necessary to exclude non-urban areas when drawing safety risk map of nighttime light environment. Moreover, land classification data of Dalian with a precision of 30 m (Data source: National Earth System Science Data Sharing Service Platform) is used in GIS software to extract horizontal illuminance inversion data of urban areas of Dalian, as shown in Figure 20.

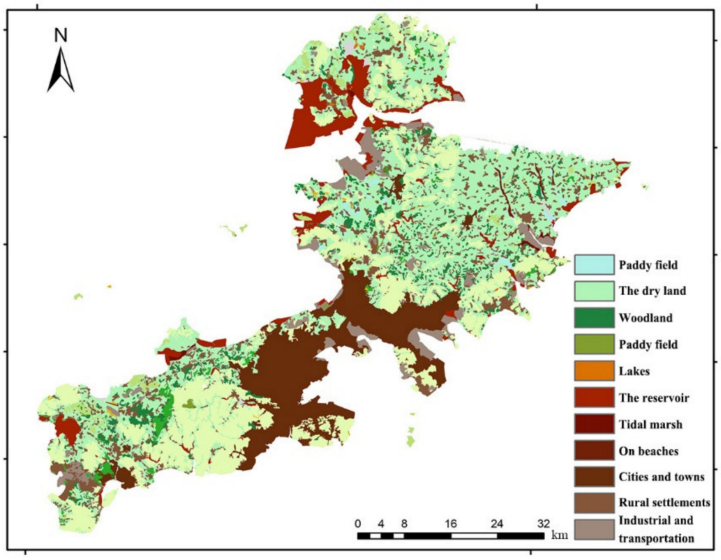

Figure 19. Land classification data of Dalian urban area.

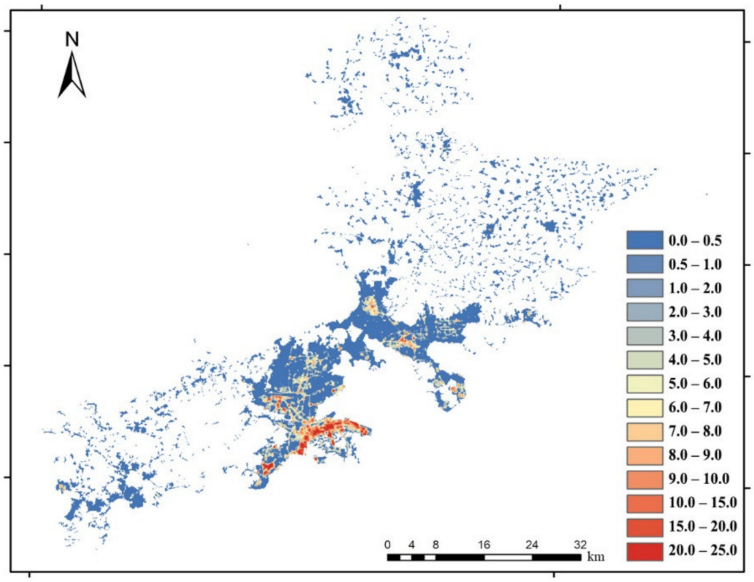

Figure 20. Inversion data of urban regional illumination in Dalian City.

Using the illuminance data of the study area, FOS questionnaire data, and environmental information data as data sources, the horizontal illuminance thresholds corresponding to different FOS levels were calculated by regression analysis. We use the illuminance thresholds corresponding to different FOS levels and the data classification tool of GIS to reclassify the ground horizontal illuminance inversion data and draw the night lighting safety map of Dalian (Figure 21). The ground horizontal illuminance inversion data are divided into four categories: the area with FOS < 1 is very unsafe, the area with $1 \leq$ FOS < 2 is slightly unsafe, the area with $2 \leq$ FOS < 3 is relatively safe, and the area with $3 \leq$ FOS is very safe.

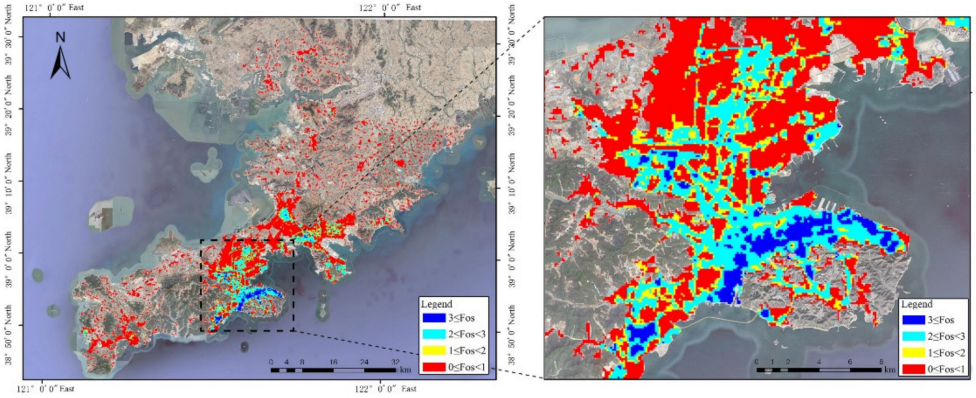

Figure 21. Safety map of night lighting in urban areas of Dalian City.

4.2. Urban Night Light Environment Risk Monitoring System Construction

The advanced technologies, such as high-precision remote sensing technology and big data analysis and processing technology, can be used to comprehensively monitor the urban night light environment, accurately locate the risk points, and timely deal with the problems, so as to build a flexible and efficient urban night light environment risk prevention and control system. In terms of monitoring, we can use the periodically updated night light remote sensing data together with the ground inversion method and the ground light environment database of this study to periodically generate the urban night light environment risk map, so as to realize the periodic monitoring of the urban night light environment and the accurate capture of risk points. The effect of light

environment treatment at night can be evaluated and compared in real time through periodic monitoring results.

4.3. Architectural Design Strategy

Through the analysis of the urban night light environment risk map, it can be found that the areas with low safety scores are mostly in urban residential areas, squares, parks and urban offshore areas. With the same urban form parameters, there are great differences in the night light environment in different areas due to the different proportion of building form, building materials, landscape and lamps. For example, the shielding of different building forms and vegetation methods for urban public lights, and the reflection of different materials on night lights can have a direct impact on the urban night light environment. Therefore, based on the current national specifications, design proposals for improving the safety of night lighting should be put forward from four aspects: architectural form layout, building materials, landscape supporting and luminaires and provide reference for architectural design strategies to reduce the area proportion of low lighting safety in urban areas and to build a high-quality urban night light environment.

5. Conclusions

In this study, Luojia-01 remote sensing data and the measured data of multi-parameter and multi-window urban night light environment were used to explore the relationship between high-precision remote sensing data and the various parameters used in the study of traditional building light environment, and the illuminance inversion model of ground night light environment is established. In the collection of ground survey data, the traditional survey method is reconstructed from three aspects, the arrangement of measurement points, the measurement window and the selection of measurement parameters. In terms of measurement point layout, the study constructed the "measurement unit" combining with the grid size of Luojia-01 remote sensing data and sets point density 4 as the optimal density to collect the measured data of three measurement Windows and three parameters of 249 measurement units in Dalian. The findings of data analysis are as follows:

(1) Spatial Distribution Characteristics of Ground Light Environment

The numerical order of the illuminance parameters of the three windows is: horizontal window > lower window > upper window; Among them, Chunliu, Heishijiao street has more than 70% of the area whose horizontal window value is more than 6 times the lower window value. The brightness value order of the three windows is horizontal window > lower window > upper window; There are four streets having 90% of each area whose brightness value of the horizontal window is more than 3 times that of the lower window. In the distribution diagram of the ratio between horizontal window and upper window, the ratio of more than 90% area is between 3–18 times. Three windows are sorted by magnitude brightness values as upper window > lower window > horizontal window; In the three windows, the mean value of light environmental parameters corresponding to each urban functional area presents relatively consistent characteristics, and the areas with high lighting degree are mainly distributed in commercial offices and square green space. The areas with low lighting levels are distributed in closed and open residential areas.

(2) Inversion Model Construction of Remote Sensing Data

In the correlation between the remote sensing data and the measured data, the correlation between the measured values of the horizontal window and the upper window of the ground illuminance parameters and the remote sensing data of Luojia-01 is the best. According to the spatial distribution characteristics of ground light environment, six traditional regression models are established to analyze the correlation between remote sensing and measured data by extracting the illuminance data and remote sensing data of horizontal window. Among them, the correlation coefficient of cubic polynomial and RMSE value of validation set are the best. This model is used to invert the illuminance at night and

draw the illuminance map of Dalian city. Compared with the original data, the inversion results have better performance in the correlation and continuity of population data.

Author Contributions: Conceptualization, M.L., B.Z. and Y.L. (Yuchuan Liu); methodology, M.L., B.Z. and Y.L. (Yuchuan Liu); software, Y.L. (Yiwei Li), L.F. and Y.L. (Yuchuan Liu); validation, Y.L. (Yiwei Li), W.J. and Y.L. (Yuchuan Liu); formal analysis, Y.L. (Yiwei li); investigation, Y.L. (Yiwei Li) and Y.L. (Yuchuan Liu)resources, Q.L.; data curation, Q.L.; writing—original draft preparation, M.L. and Y.L. (Yiwei Li); writing—review and editing, M.L., B.Z., W.J. and Q.L.; visualization, M.L., T.L., L.F. and Q.L.; supervision, M.L., B.Z. and Y.L. (Yuchuan Liu); and funding acquisition, M.L. All authors have read and agreed to the published version of the manuscript.

Funding: This research was funded by National Key Research and Development Program of China, grant number 2017YFE0125900 and The National Natural Science Foundation of China, grant number 52178067.

Acknowledgments: The authors thank editors and three anonymous reviewers for their valuable comments to improve our manuscript. We give thanks to the Hubei Data and Application Center of the High-Resolution Earth Observation System for providing Luojia 1-01 data.

Conflicts of Interest: The authors declare no conflict of interest.

References

1. Raap, T.; Sun, J.; Pinxten, R.; Eens, M. Disruptive effects of light pollution on sleep in free-living birds: Season and/or light intensity-dependent. *Behav. Process.* **2017**, *144*, 13–19. [CrossRef] [PubMed]
2. Kloog, I.; Haim, A.; Stevens, R.G.; Portnov, B.A. Global Co-Distribution of Light at Night (LAN) and Cancers of Prostate, Colon, and Lung in Men. *Chronobiol. Int.* **2009**, *26*, 108–125. [CrossRef] [PubMed]
3. Riegel, K.W. Light pollution. *Science* **1973**, *179*, 1285–1291. [CrossRef] [PubMed]
4. Kyba, C.C.M.; Kuester, T.; Sanchez De Miguel, A.; Baugh, K.; Jechow, A.; Hoelker, F.; Bennie, J.; Elvidge, C.D.; Gaston, K.J.; Guanter, L. Artificially lit surface of Earth at night increasing in radiance and extent. *Sci. Adv.* **2017**, *3*, e1701528. [CrossRef]
5. Ispas, N.; Trusca, D. Urban planning and traffic safety at night. In Proceedings of the IOP Conference Series-Materials Science and Engineering, Iasi, Romania, 9–10 June 2016.
6. Tahar, M.R.; Kamarudin, F.; Umar, R.; Kamarudin, M.K.A.; Sabri, N.H.; Ahmad, K.; Rahim, S.A.; Baharim, M.S.A. Spatial Model of Sky Brightness Magnitude in Langkawi Island, Malaysia. *Res. Astron. Astrophys.* **2017**, *17*, 037. [CrossRef]
7. Liu, M.; Yang, L. Comparison and Analysis of the Light Pollution Effect at Night in the Typical Commercial Areas of Milan and Dalian. *China Illum. Eng. J.* **2020**, *31*, 94–101.
8. Puschnig, J.; Naeslund, M.; Schwope, A.; Wallner, S. Correcting sky-quality-meter measurements for ageing effects using twilight as calibrator. *Mon. Not. R. Astron. Soc.* **2021**, *502*, 1095–1103. [CrossRef]
9. Kollath, Z.; Szaz, D.; Kollath, K.; Tong, K.P. Light Pollution Monitoring and Sky Colours. *J. Imaging* **2020**, *6*, 104. [CrossRef]
10. Butt, M.J. Estimation of Light Pollution Using Satellite Remote Sensing and Geographic Information System Techniques. *GISci. Remote Sens.* **2012**, *49*, 609–621. [CrossRef]
11. Netzel, H.; Netzel, P. High resolution map of light pollution over Poland. *J. Quant. Spectrosc. Radiat. Transf.* **2016**, *181*, 67–73. [CrossRef]
12. Small, C.; Elvidge, C.D. Night on Earth: Mapping decadal changes of anthropogenic night light in Asia. *Int. J. Appl. Earth Obs.* **2013**, *22*, 40–52. [CrossRef]
13. Jiang, W.; He, G.; Long, T. Using Time Series Nighttime Images to Measure Light Pollution Trend in China. *Int. J. Environ. Sci. Dev.* **2017**, *8*, 622–625. [CrossRef]
14. Zhang, G.; Li, L.; Jiang, Y.; Shen, X.; Li, D. On-Orbit Relative Radiometric Calibration of the Night-Time Sensor of the LuoJia1-01 Satellite. *Sensors* **2018**, *18*, 4225. [CrossRef]
15. Hao, Q. Research on Digital Observation and Spatial Model Construction of Multi-Dimensional Urban Nighttime Light Environment. Master's Thesis, Dalian University of Technology, Dalian, China, 2019.
16. Aube, M.; Simoneau, A. New features features to the night sky radiance model illumina: Hyperspectral support, improved obstacles and cloud reflection. *J. Quant. Spectrosc. Radiat. Transf.* **2018**, *211*, 25–34. [CrossRef]
17. Roychowdhury, K.; Jones, S.D.; Arrowsmith, C.; Reinke, K. A Comparison of High and Low Gain DMSP/OLS Satellite Images for the Study of Socio-Economic Metrics. *IEEE J. Sel. Top. Appl. Earth Obs. Remote Sens.* **2011**, *4*, 35–42. [CrossRef]
18. Katz, Y.; Levin, N. Quantifying urban light pollution—A comparison between field measurements and EROS-B imagery. *Remote Sens. Environ.* **2016**, *177*, 65–77. [CrossRef]
19. Li, J.; Xu, Y.; Cui, W.; Ji, M.; Su, B.; Wu, Y.; Wang, J. Investigation of Nighttime Light Pollution in Nanjing, China by Mapping Illuminance from Field Observations and Luojia 1-01 Imagery. *Sustainability* **2020**, *12*, 681. [CrossRef]
20. Liao, Z. Research on Land Surface Temperature Inversion Based on Surface Sensor Data and Remote Sensing Data. Master's Thesis, China University of Mining and Technology, Beijing, China, 2014.

21. Kuechly, H.U.; Kyba, C.C.M.; Ruhtz, T.; Lindemann, C.; Wolter, C.; Fischer, J.; Hoelker, F. Aerial survey and spatial analysis of sources of light pollution in Berlin, Germany. *Remote Sens. Environ.* **2012**, *126*, 39–50. [CrossRef]
22. Tan, H.; Liu, P.; Li, B. Perception of Tourism Destination Image in Dalian Based on Network Text Analysis. *Econ. Geogr.* **2021**, *41*, 231–239.
23. Hubei Data and Application Network. Available online: http://www.hbeos.org.cn (accessed on 1 August 2019).
24. The Luojia-La Scientific Experimental Satellite was Successfully Launched. Available online: http://www.lmars.whu.edu.cn/index.php/en/researchnews/2169.html (accessed on 1 August 2019).
25. Jiang, W.; He, G.; Long, T.; Guo, H.; Yin, R.; Leng, W.; Liu, H.; Wang, G. Potentiality of Using Luojia 1-01 Nighttime Light Imagery to Investigate Artificial Light Pollution. *Sensors* **2018**, *18*, 2900. [CrossRef]
26. Jiang, P.; Zeng, Z.; Chen, J.; Huang, T. Generalized Regression Neural Networks with K-Fold Cross-Validation for Displacement of Landslide Forecasting. In *Advances in Neural Networks, Proceedings of the International Symposium on Neural Networks, Hong Kong, China, 28 November–1 December 2014*; Springer: Cham, Switzerland, 2014; pp. 533–541.
27. Freire, A.L.; Rocha-Neto, A.R.; Barreto, G.A. On robust randomized neural networks for regression: A comprehensive review and evaluation. *Neural Comput. Appl.* **2020**, *32*, 16931–16950. [CrossRef]
28. Dailian Municipal Bureau of Statistics. Available online: https://stats.dl.gov.cn/col/col3811/index.html (accessed on 1 August 2019).
29. Li, Y.; Chen, A.; Zhou, Y.; Zou, N.; He, X.; Wang, J. Research on the assessment indicators for crime prevention lighting in residential areas based on AHP and Entropy Weight. In Proceedings of the MATEC Web of Conferences, Amsterdam, The Netherlands, 28 June 2016.
30. Fotios, S.; Unwin, J.; Farrall, S. Road lighting and pedestrian reassurance after dark: A review. *Lighting Res. Technol.* **2015**, *47*, 449–469. [CrossRef]